Gilabert, V., et al., 2021, Contribution of orbital forcing and Deccan volcanism to global climatic and biotic changes across the Cretaceous-Paleogene boundary at Zumaia, Spain: Geology, v. 49, https://doi.org/10.1130/G49214.1

SUPPLEMENTARY MATERIAL

Contribution of orbital forcing and Deccan volcanism to global climatic and biotic changes across the KPB at Zumaia, Spain

Vicente Gilabert[1], Sietske J. Batenburg[2], Ignacio Arenillas[1], José A. Arz[1]

[1]Departamento de Ciencias de la Tierra-IUCA, Universidad de Zaragoza, E-50009 Zaragoza, Spain.

[2] Departament de Dinàmica de la Terra i de l'Oceà, Facultat de Ciències de la Terra, Universitat de Barcelona, 08028 Barcelona, Spain.

This Supplemental Material contains:

Text S1: Detailed Methodology.

Text S2: Geochemical and geophysical properties.

Text S3: Age models.

Text S4: Stratigraphic continuity across the KPB at Zumaia.

Supplementary figures S1-S5.

Supplementary Tables S1-S5 (in a separate supplementary data file named: Supplementary Tables S1-S5_Gilabert_et_al.xlsx.)

Supplementary references cited.

Text S1: Detailed Methodology

Sampling: For the micropaleontological, geochemical and geophysical analysis, we sampled 24.5 m across the Cretaceous/Paleogene boundary (KPB) of the Zumaia section. A total of 171 samples were taken, of which 103 samples were from the 16-m-thick Maastrichtian interval and 68 from the 8.5-m-thick Danian interval. The sample spacing for the Maastrichtian was of 15–20 cm, except for the 2 m below the KPB, which were sampled every 5–10 cm. The Danian interval was sampled every 2.5–5 cm across the first 80 cm and every 15 cm further upwards.

Micropaleontology: We follow the disaggregating technique of Lirer (2000) which employs dilute acetic acid for 3-4 hours to liberate calcareous microfossils from strongly lithified calcareous rocks such as those from Zumaia. The disaggregated samples were then washed through a 63 µm sieve and oven-dried at 50 ºC. When quantitative analysis was possible, the samples were split with a microsplitter to obtain a representative aliquot of ca. 300 specimens per sample.

Calcium carbonate content: The calcium carbonate content of each rock sample was estimated with a manocalcimeter by measuring and recording the carbon dioxide pressure rise produced by acid attack on the rock sample. 171 rock samples were analyzed, which were mechanically powdered to avoid the secondary calcite veins. The analyses were performed by adding 5ml of 5M HCl to one gram of powdered sample in the reaction cell, which is independent of the atmospheric pressure.

Carbon isotope analyses: Measurements of $\delta^{13}C$ were performed on homogenized bulk powdered sediment from the same 171 samples. Samples were analyzed in the Department of Earth Sciences of the University of Oxford, using a GasBench device attached to a ThermoFisher Delta V Advantage gas source isotope ratio mass spectrometer. Carbon isotopes are reported using the standard delta notation ($\delta^{13}C$) in parts per mill (‰) on the Vienna PeeDee Belemnite (VPDB) scale. Calibration of samples to the VPDB scale was achieved using multiple analyses of an in-house standard. For the $\delta^{13}C$, the in-house standard, NOCZ, has an average value of 2.18‰. The NOCZ standard was calibrated to the VPDB scale by comparison with analyses of NBS-19 and NBS-18, which were assigned values of +1.95‰ and -5.014‰, respectively. Repeated analyses of in-house standards suggest a reproducibility (±1σ) of <0.1.

Magnetic susceptibility: The magnetic susceptibility (MS) of the 171 samples was measured at the University of Zaragoza, Spain, with a Kappabridge KLY-35 spinning specimen magnetic susceptibility anisotropy meter. Samples were crushed in an agate mortar and measured in cylindrical plastic boxes 10 cm^3 in volume. MS values are reported relative to mass (m^3/kg).

Text S2: Geochemical and geophysical properties.

The $\delta^{13}C$, $CaCO_3$ and magnetic susceptibility data from Zumaia presented here (Figs. 3, S2 and Table S2) are comparable to previous studies from the KPB interval at Zumaia (e.g., Batenburg et al., 2012; Dinarés-Turell et al., 2003, 2014). Fig. S2 shows that $\delta^{13}C$ and $CaCO_3$ exhibit a limited degree of correlation, although this is variable through the section. Covariation of $\delta^{13}C$ and carbonate content at the KPB and the first 50 cm of the Danian is ascribed to the KPB mass extinction that caused the decimation of the marine calcifiers, causing a sudden decrease in carbonate production (Smit, 1982; Bown, 2005; Henehan et al., 2019). The generally poor correlation in the 1 m.y. across the KPB suggests that the lithology of the Zumaia section is not the dominant control on $\delta^{13}C$ values, which is consistent with reported carbonate concentrations and $\delta^{13}C$ values for the Late Cretaceous and early Danian (e.g., Hull et al., 2020). A strong negative correlation between magnetic susceptibility and $CaCO_3$ content (Fig. S2) suggests that variations in the original fluxes of detrital material and carbonate were the main driver of variations in the concentration of paramagnetic minerals. Although we could not replicate the detailed sampling of Danian rocks of ten Kate and Sprenger (1993) due to coastal erosion, previous studies indicate that the thin layers in between indurated Danian limestones beds are marls (e.g., ten Kate and Sprenger, 1993; Dinares-Turell et al., 2003, 2014; Hilgen et al., 2010, 2015). Rather than dissolution of $CaCO_3$, the formation of marls was likely driven by increases in siliciclastic input during extremes of the precessional cycle, in a time of overall low production of $CaCO_3$ in the aftermath of the extinction of marine calcifiers at the KPB (e.g., Smit, 1982; Bown, 2005; Schulte et al., 2010).

Text S3: Age models

The age model presented here is based on the identification of the 405 k.y. component of eccentricity-modulated precession in the lithological alternations at Zumaia, following the studies by Batenburg et al. (2012) for the Maastrichtian interval and by Dinarès-Turell et al. (2014) for the Danian interval, anchored to a KPB age of 66.001 Ma, as in the 405 k.y. age model of Dinarès-Turell et al. (2014) (Table S1). The 405 k.y. periodicity, also known as long eccentricity, is the only reliable tuning target beyond 52 Ma (Laskar et al., 2011). Lithological patterns are tied to eccentricity minima and maxima, with maximal lithological contrast taken to reflect eccentricity maxima, and minimal contrast between lithologies considered to reflect eccentricity minima. Lithological alternations, i.e. limestone-marl couplets or more gradual variations in lithology, were interpreted to reflect precession-driven cyclicity (manuscript Fig. 2), following the work of Dinarès-Turell et al. (2014), Hilgen et al. (2015) and Batenburg et al. (2012). In between tie-points, precessional cycles were ascribed ages by assuming an equal duration per precessional cycle (Table S2), an approximation which allows considerable differences in sedimentation rate within 405 k.y. cycles to be accounted for. This approach is in line with that of Batenburg et al. (2012) in providing astronomically calibrated ages for bio-, chemo- and magneto-stratigraphic events.

To correlate and compare the $\delta^{13}C$ curve of Zumaia with data from other localities (ODP 1262, South Atlantic; ODP 1049 and IODP U1403, North Atlantic; and Gubbio, Italy), we anchored the $\delta^{13}C$ curves to the same KPB age, aligned the different tie-points in each locality (Table S5), and assumed a constant sedimentation rate between the tie-points.

Text S4: Stratigraphic continuity across the KPB at Zumaia

The Zumaia section was designated one of the auxiliary sections of the GSSP for the base of the Danian due to its continuity and good exposure (Molina et al., 2009). The KPB is easily identifiable at Zumaia because there is an abrupt change of facies from the uppermost Maastrichtian reddish marls to the KPB blackish clay bed (Fig. S1B). The first 2 cm of the Danian exhibits calcite veins as the result of small-scale tectonic shear stress at the Maastrichtian/Danian contact (Fig. S1B), which favored the growth of millimetric to centimetric fractures filled with calcite. Nevertheless, moving laterally across the outcrop, sites can be found where the KPB sequence is better exposed and is less affected by calcite veins. At Zumaia, the KPB is well marked by a millimeter-thick airfall layer consisting of altered microtektites, referred to as microkrystites by Smit (1999), and a “rusty” layer (Fig. S1C-E). According to Smit (1990), the airfall layer at Zumaia has an anomalous iridium concentration of up to 26.3 ppb, which is similar to other iridium anomalies identified in well-known KPB sections such as Caravaca (Smit, 1982) and Agost (Ruíz et al., 1992). At Zumaia, the mass extinction horizon of planktic foraminifera coincides with the airfall layer at the base of the KPB Clay (Fig. S3).

Our lithological, cyclostratigraphic, micropaleontological and geochemical observations refute the recent suggestion by Font et al. (2018) that there would be a ~150 k.y. hiatus across the KPB. Above and below the boundary clay, rhythmic alternations of marls and limestones at Zumaia have proven instrumental for the tuning and correlation of sections worldwide (ten Kate and Sprenger, 1993; Westerhold et al., 2008; Batenburg et al., 2012; Dinares-Turell et al., 2014; Hilgen et al., 2015; this work), and even for intercalibrating astrochronology and radiometric dating (Kuiper et al., 2008). We recognized 13.5 precession cycles in the ~ 4-m-thick interval between the KPB and the C29r/C29n reversal, which represents the first ~300 k.y. of the Danian, in line with previous cyclostratigraphic studies for this interval at Zumaia (Dinarès-Turell et al., 2003, 2014; Hilgen et al., 2010, 2015). A hiatus of ~150 k.y. as proposed by Font et al. (2018) implies that the lithological alternations only represent 6–7 precession cycles with an average thickness of ~0.6 m per precession cycle, similar to lithological couplets in the Maastrichtian (~0.7 m average thickness; Batenburg et al., 2012). Such a low number of cycles is not in agreement with the bedding patterns, and a constant sedimentation rate is not in agreement with the change in lithology from predominantly marl in the uppermost Maastrichtian to predominantly limestone in the lowermost Danian at Zumaia, ascribed to a sharp drop in siliciclastic supply (Dinarès-Turell et al., 2003). Abrupt changes in sedimentation rate are commonly recognized at other localities in the early Danian (e.g., Smit, 1999; D'Hondt et al., 2005; Dameron et al., 2017).

Unlike the biostratigraphic study of Font et al. (2018), we were able to recognize the complete sequence of biozones and bioevents of planktic foraminifera across the KPB interval of Zumaia. For the Maastrichtian, these include the lowest occurrence datum (LOD) of *Plummerita hantkeninoides* and the highest occurrence datum (HOD) of *Archaeoglobigerina cretacea* (Fig. S3, Tables S3 and S4), in stratigraphic positions directly correlatable to those recognized in other reference sections such as El Kef (Tunisia; Arenillas et al., 2000a), Aïn Setara (Tunisia; Arenillas et al., 2000b), Caravaca (Spain; Gilabert et al., 2021), and Agost (Spain; Molina et al., 2005). All the lowermost Danian biozones of Arenillas et al. (2004) and Wade et al. (2011) and all the planktic foraminiferal acme-stages (PFAS) of Arenillas et al. (2006) are identified in this section (Figs. 2, 3, S2, S3, S4, Tables S3 and S4). The PFAS have been reported worldwide, mainly in the Tethys, North Atlantic and Gulf of Mexico-Caribbean regions (Arenillas et al., 2000a,b, 2018; Alegret et al., 2004; Gallala et al., 2009; Renne et al., 2018; Lowery et al., 2018), and consequently they have been considered a very useful tool for biostratigraphic correlation. Their identification in the lowermost Danian provides additional support in assessing the stratigraphic continuity of the Zumaia section across the KPB. Danian nannoplankton assemblages typically display a similar acme stage sequence worldwide (e.g., Jiang et al., 2010; Jones et al., 2019; Gibbs et al., 2020), which has been recognized at Zumaia by Bernaola et al. (2006) above the KPB (Table S2).

The geochemical and isotope-stratigraphic record at Zumaia also supports the completeness of the stratigraphic record. We recognize all the isotopic events identified worldwide across the KPB (see main text), including the sharp decrease in $CaCO_3$ and $\delta^{13}C$ that is recognized worldwide (Molina et al., 2009; Schulte et al., 2010; Sepulveda et al., 2019; Fig. 3 and Table S2).

Supplementary figures S1-S5

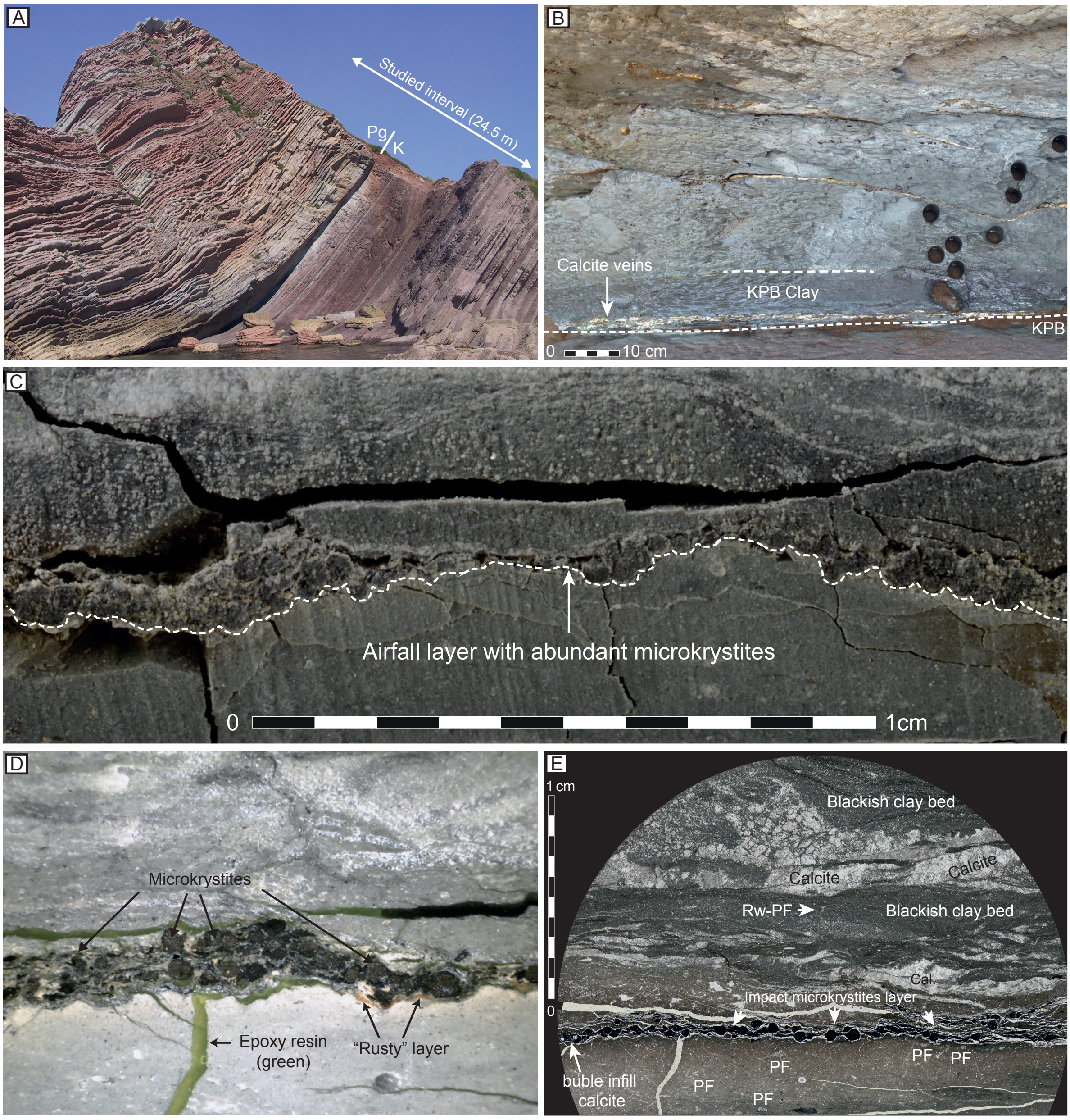

Figure S1: Cretaceous-Paleogene transition of Zumaia at different scales. A) Field overview of the Zumaia outcrop, illustrating the rhythmic lithological patterns across the upper Maastrichtian (reddish-marl-dominated upper part of the Zumaia-Algorri Formation) and lower Danian (limestone-dominated lower part of the Aitzgorri Formation). B) Detailed field view of the boundary interval; the KPB is located at the base of the KPB Clay. C) Magnified view of the airfall layer with abundant microkrystites in concordant contact with the underlying Maastrichtian sediments. D) Detail of ejecta-rich airfall layer, illustrating lateral changes in thickness. E) Thin-section micrograph of the airfall layer under a petrographic microscope; several *in situ* planktic foraminifera specimens in the reddish Maastrichtian marls can also be recognized, and only one reworked specimen in the overlying blackish clay bed.

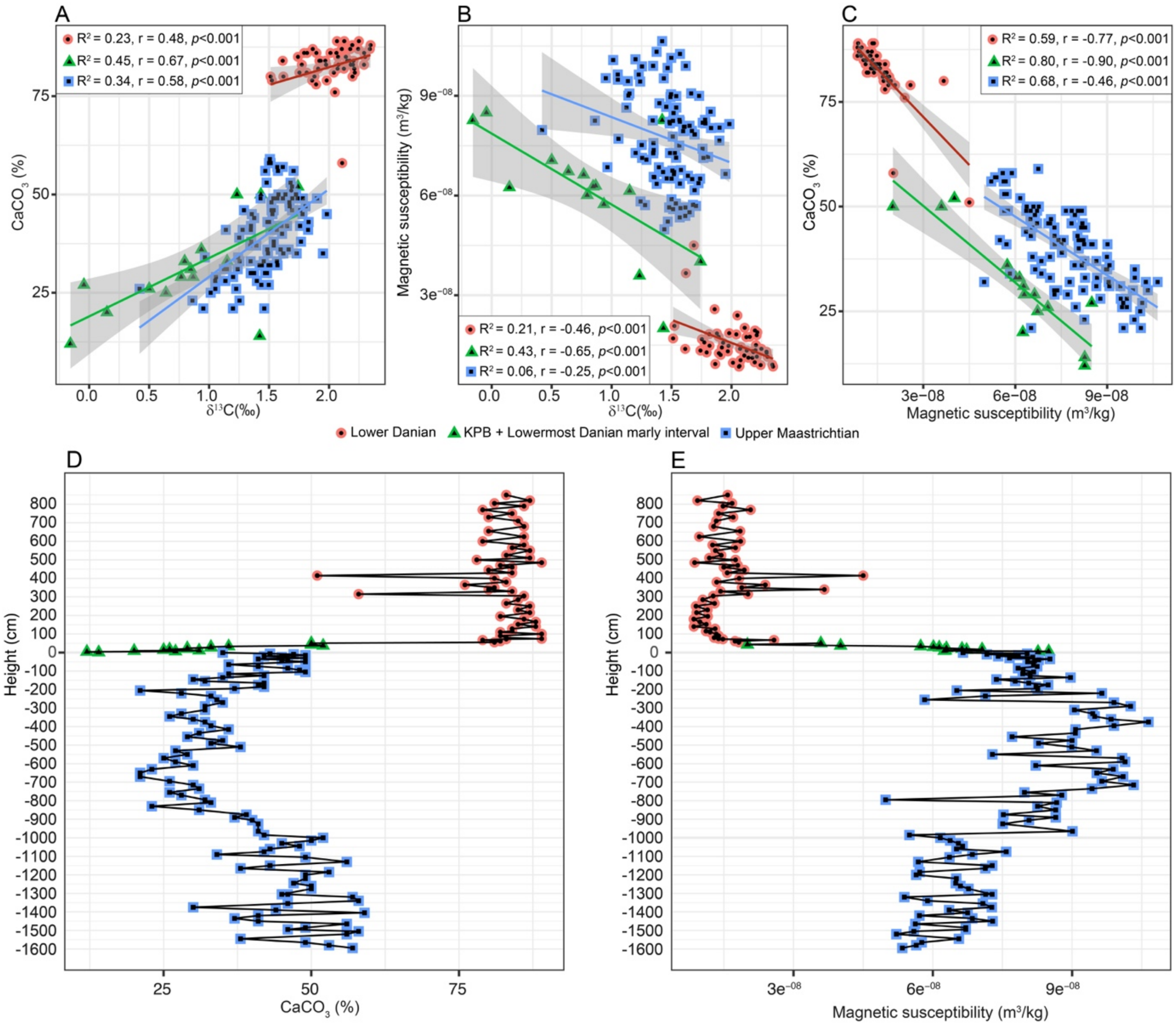

Figure S2: Cross-plots between $CaCO_3$ and $\delta^{13}C$ (A), magnetic susceptibility and $\delta^{13}C$ (B), $CaCO_3$ and magnetic susceptibility, the gray shadow in each plot represents the standard error. Changes in the values of $CaCO_3$ (D) and magnetic susceptibility (E) across the Zumaia section.

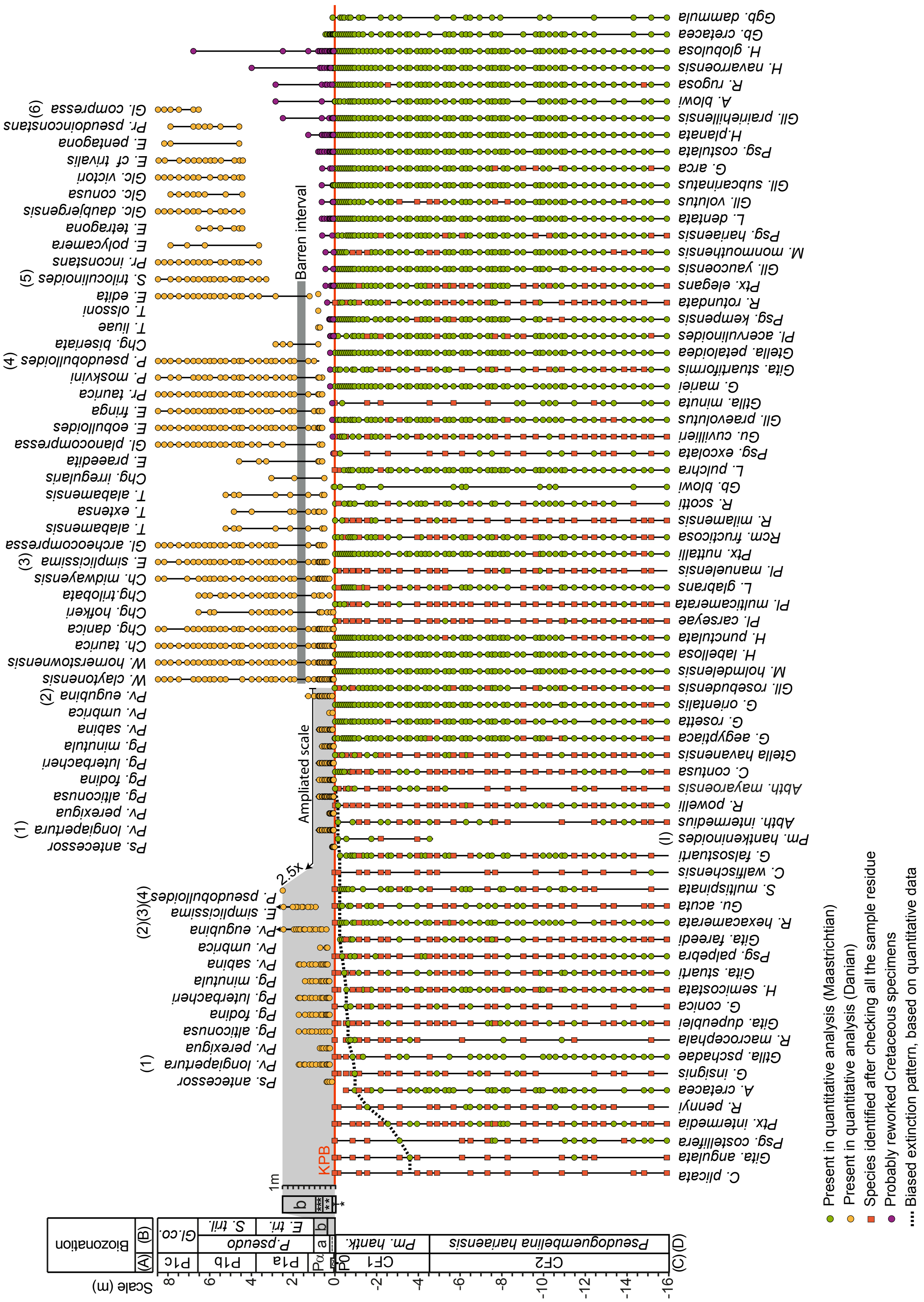
Present in quantitative analysis (Maastrichtian)
Present in quantitative analysis (Danian)
Species identified after checking all the sample residue
Probably reworked Cretaceous specimens
Biased extinction pattern, based on quantitative data
Barren interval
Ampliated scale
2.5x
KPB
1m
Biozonation
Scale (m)
Pseudoguembelina hariaensis
Pm. hantk.
P.pseudo
CF2
CF1
P0
P1a
P1b
P1c

Figure S3: Stratigraphic ranges of the late Maastrichtian and early Danian planktic foraminiferal species recognized at the Zumaia section. Dashed line represents the extinction pattern based only on quantitative data, showing a biased extinction pattern. Lowest occurrence datums (LODs) of the species numbered from (1) to (6) are the base of the biozones and subbiozones of Arenillas et al. (2004). (I) LOD of *Plummerita hantkeninoides* is the base of the uppermost Maastrichtian Biozone CF1 of Li and Keller (1998). Biozonations: A – Wade et al. (2011); B – Arenillas et al. (2004); C – Li and Keller (1998); D – Arz and Molina (2002). C– *Contusotruncana*; Gita– *Globotruncanita*; Psg.– *Pseudoguembelina*; R. *Rugoglobigerina*; A–*Archaeoglobigerina*; G.–*Globotruncana*; Gtlla.– *Globotruncanella*; H.–*Heterohelix*; Gu.–*Gublerina*; S.–*Schackoina*; Pm.–*Plummerita*; Abth.– *Abathomphalus*; Gll.–*Globigerinelloides*; M.–*Muricohedbergella*; Pl.–*Planoglobulina*; L.– *Laeviheterohelix*; Ptx.–*Pseudotextularia*; Rcm.– *Racemiguembelina*; Gb.–*Guembelitria* for the Maastrichtian. Ps.–*Pseudocaucasina*; Pv.–*Parvularugoglobigerina*; Pg.– *Palaeoglobigerina*; E.–*Eoglobigerina*; P.–*Parasubbotina*; W.–*Woodringina*; Ch.– *Chiloguembelina*; Chg.– *Chiloguembelitria*; Gl.–*Globanomalina*; T.–*Trochoguembelitria*; Pr.–*Praemurica*; S.–*Subbotina*; Glc.–*Globoconusa* for the Danian.

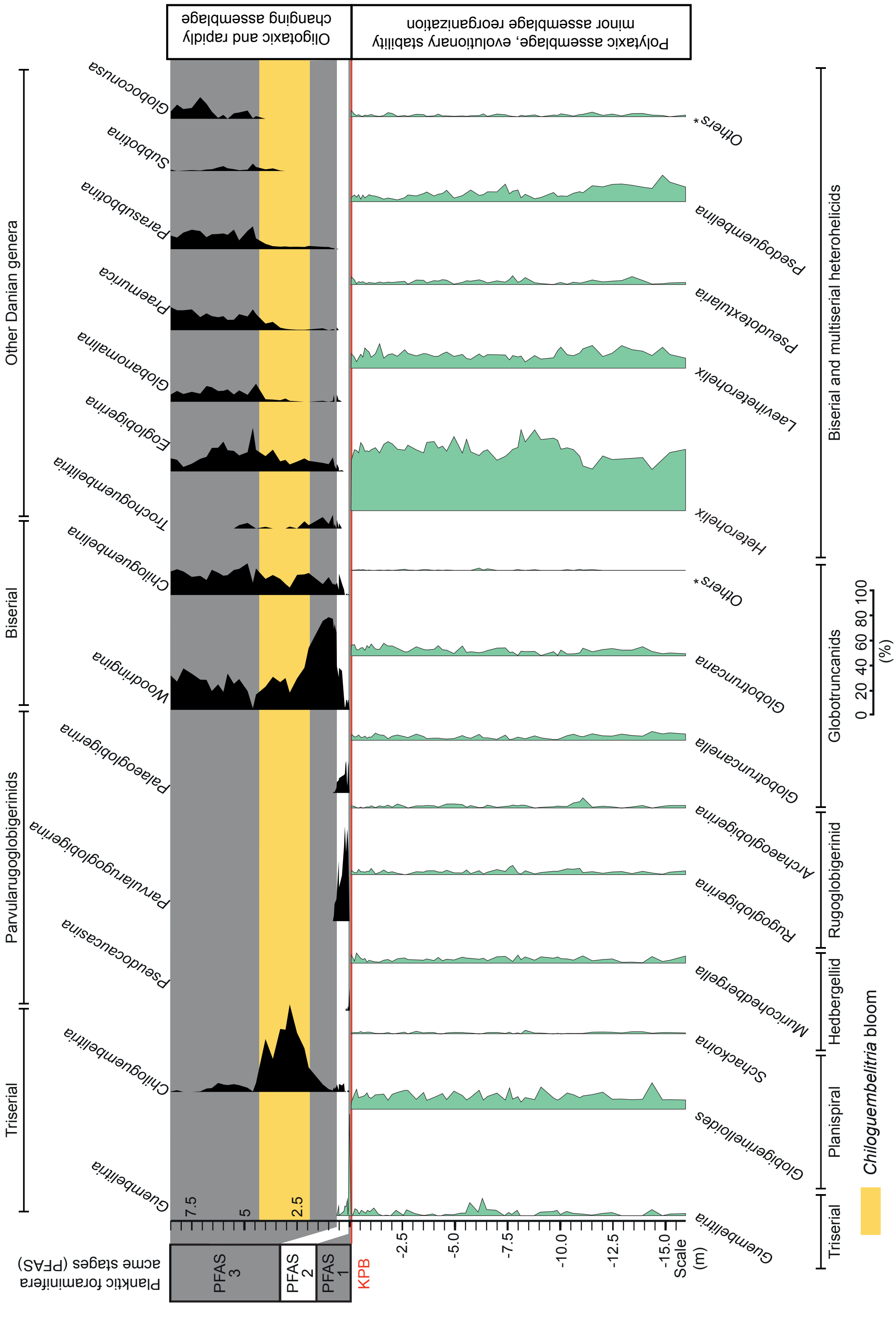

Figure S4: Quantitative analysis of planktic foraminifera based on the >63 microns sieved fraction. (Others* Globotrunanids) – *Abathomphalus* + *Contusotruncana* +*Globotruncanita*; (Others* Biserial and multiserial heterohelicids) – *Racemiguembelina* + *Planoglobulina* + *Gublerina.*

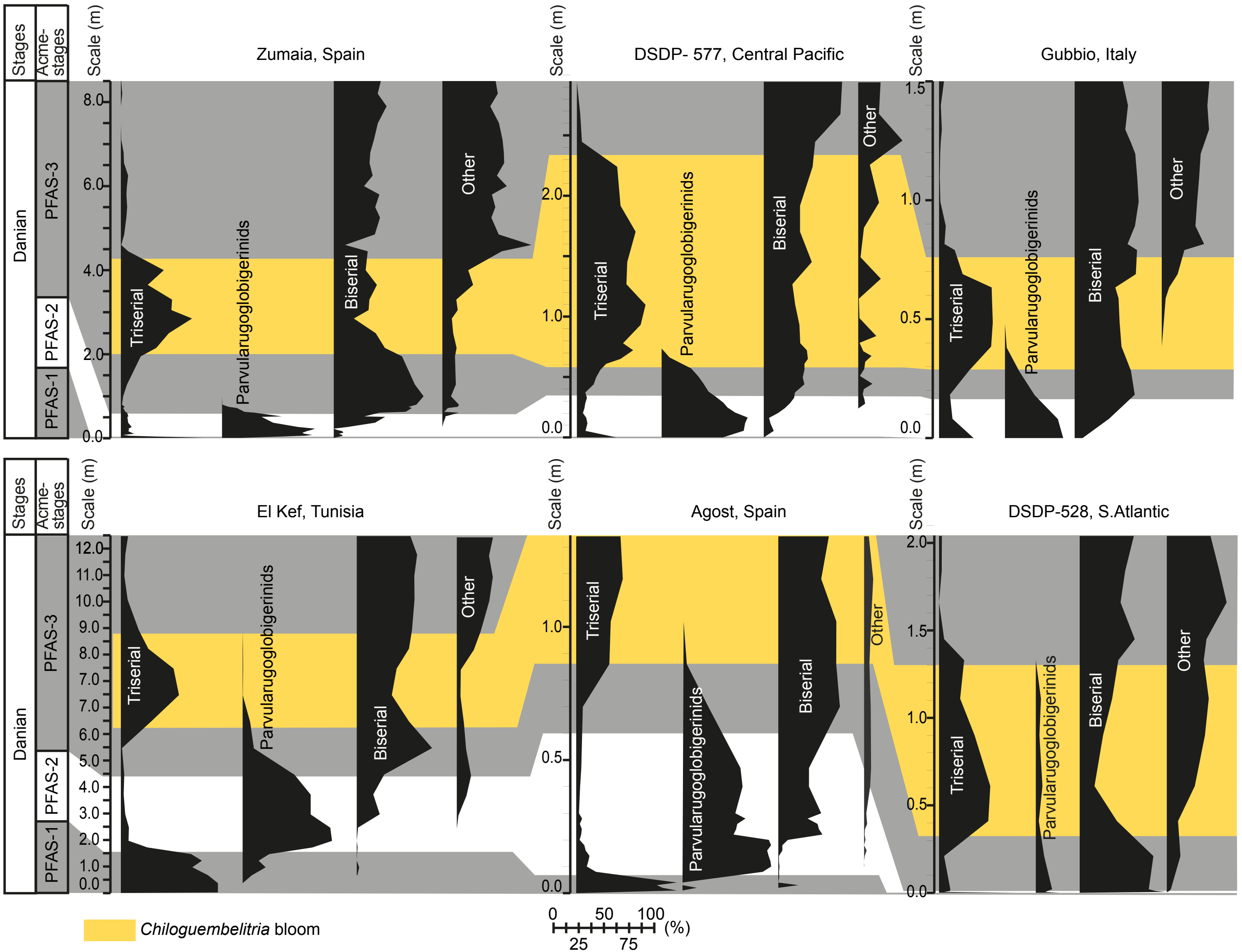

Stages
Acme-stages
Scale (m)
Zumaia, Spain
DSDP- 577, Central Pacific
Gubbio, Italy
El Kef, Tunisia
Agost, Spain
DSDP-528, S.Atlantic
Danian
PFAS-1
PFAS-2
PFAS-3
Triserial
Parvularugoglobigerinids
Biserial
Other
0 25 50 75 100 (%)
Chiloguembelitria bloom

Figure S5: Correlation of the lowermost Danian PFAS at Zumaia (this study), El Kef (Tunisia; Arenillas et al., 2018), DSDP-577 (Central Pacific; Smit and Romein, 1985), Agost (Spain; Canudo et al., 1991), Gubbio (Italy; Coccioni et al., 2010) and DSDP 528 (South Atlantic; D´Hondt and Keller, 1991). Triserial taxa = *Guembelitria* and *Chiloguembelitria*. Parvularugoglobigerinids (tiny trochospiral taxa): *Parvularugoglobigerina* and *Palaeoglobigerina*. Biserial taxa: *Woodringina* and *Chiloguembelina*. Other taxa: *Eoglobigerina*, *Parasubbotina*, *Subbotina*, *Globanomalina* and *Praemurica* (*Trochoguembelitria* and *Globoconusa* are also included here).

Supplementary Tables S1-S5

(Tables S1-S5 are in a separate supplementary data file named: Supplementary Tables S1-S5_Gilabert_et_al.xlsx.)

Table S1: Tie-points for the astronomically calibrated age model of the Cretaceous-Paleogene transition at Zumaia. Min.–Minima; max.–maxima. All the ages are based on the La2011 astronomical solution (Laskar et al., 2011); the KPB age is based on the 405 k.y. calibration by Dinarès-Turell et al. (2014); the 405 eccentricity maxima follow the nomenclature of Husson et al. (2011).

Table S2: Astronomically calibrated age model for the Cretaceous-Paleogene transition at Zumaia.

Table S3: Relative abundance of planktic foraminiferal species in the upper Maastrichtian of Zumaia.

Table S4: Relative abundance of planktic foraminiferal species in the lower Danian of Zumaia.

Table S5: Age model tie-points for other Cretaceous-Paleogene sections. All the ages are based on the La2011 astronomical solution (Laskar et al., 2011); the KPB age is based on the 405 k.y. eccentricity calibration of Dinarès-Turell et al. (2014); the 405 eccentricity maxima follow the nomenclature of Husson et al. (2011). The ages for KPB and C29r/C29n are based on the astronomical tuning of Dinarès-Turell et al. (2014). The age for the $\delta^{13}C$ minimum below C30n/C29r is based on the astronomical tuning of Batenburg et al. (2018). min.–Minima; max.–maxima.

Supplementary references cited

Alegret, L., Arenillas, I., Arz, J.A., and Molina, E., 2004, Foraminiferal event-stratigraphy across the Cretaceous/Tertiary boundary: Neues Jahrbuch für Geologie und Paläontologie, Abhundlungen, v. 234, no. 1-3, p. 25–50, https://doi.org/0.1127/NJGPA/234/2004/25.

Arenillas, I., Arz, J.A., Molina, E., and Dupuis, C., 2000a, An independent test of planktonic foraminiferal turnover across the Cretaceous/Paleogene (K/P) boundary at El Kef, Tunisia: Catastrophic mass extinction and possible survivorship: Micropaleontology, v. 46, p. 31–49.

Arenillas, I., Arz, J.A., Molina, E., and Dupuis, C., 2000b, The Cretaceous/Paleogene (K/P) boundary at Aïn Settara, Tunisia: sudden catastrophic mass extinction in planktic foraminifera: Journal of Foraminiferal Research, v. 30, p. 202–218, https://doi.org/10.2113/0300202.

Arenillas, I., Arz, J.A., and Molina, E., 2004, A new high-resolution planktic foraminiferal zonation and subzonation for the lower Danian: Lethaia, v. 37, p. 79–95, https://doi.org/10.1080/00241160310005097.

Arenillas, I., Arz, J.A., Grajales-Nishimura, J.M., Murillo-Muñetón, G., Alvarez, W., Camargo-Zanoguera, A., Molina, E., and Rosales-Domínguez, C., 2006, Chicxulub impact event is Cretaceous/Paleogene boundary in age: New micropaleontological evidence: Earth and Planetary Science Letters, v. 249, p. 241–257, https://doi.org/10.1016/j.epsl.2006.07.020.

Arenillas, I., Arz, J.A., and Gilabert, V., 2018, Blooms of aberrant planktic foraminifera across the K/Pg boundary in the Western Tethys: Causes and evolutionary implications: Paleobiology, v. 44, p. 460–489, https://doi.org/10.1017/pab.2018.16

Arz, J.A., and Molina, E., 2002, Bioestratigrafía y cronoestratigrafía con foraminíferos planctónicos del Campaniense superior y Maastrichtiense de latitudes subtropicales y templadas (España, Francia y Tunicia): Neues Jahrbuch für Geologie und Paläontologie, Abhandlungen, v. 224, p. 161–195, https://doi.org/ 10.1127/njgpa/224/2002/161.

Batenburg, S.J. et al., 2012, Cyclostratigraphy and astronomical tuning of the Late Maastrichtian at Zumaia (Basque country, Northern Spain): Earth and Planetary Science Letters, v. 359–360, p. 264–278, https://doi.org/10.1016/j.epsl.2012.09.054.

Batenburg, S.J. et al., 2018, Late Maastrichtian carbon isotope stratigraphy and cyclostratigraphy of the Newfoundland Margin (Site U1403, IODP Leg 342): Newsletters on Stratigraphy, v. 51, p. 245–260, https://doi.org/10.1127/nos/2017/0398.

Bernaola G., Baceta J.I., Payros A., Orue-Etxebarria X. and Apellaniz E., 2006. The Paleocene and lower Eocene of the Zumaia section (Basque Basin): *in* Climate and Biota of the Early Paleogene 2006. Post Conference Field Trip Guidebook, Bilbao, Spain 82 p.

Bown, P., 2005, Selective calcareous nannoplankton survivorship at the Cretaceous-Tertiary boundary: Geology, v. 33, p. 653–656, doi:10.1130/G21566.1.

Canudo, J.I., Keller, G., and Molina, E., 1991, Cretaceous/Tertiary boundary extinction pattern and faunal turnover at Agost and Caravaca, S.E. Spain: Marine Micropaleontology, v. 17, p. 319–341, https://doi.org/10.1016/0377-8398(91)90019-3.

Coccioni, R., and Silva, I.P., 2015, Revised upper Albian-Maastrichtian planktonic foraminiferal biostratigraphy and magneto-stratigraphy of the classical tethyan Gubbio section (Italy): Newsletters on Stratigraphy, v. 48, p. 47–90, https://doi.org/10.1127/nos/2015/0055.

Coccioni, R., Frontalini, F., Bancalà, G., Fornaciari, E., Jovane, L., and Sprovieri, M., 2010, The Dan-C2 hyperthermal event at Gubbio (Italy): Global implications, environmental effects, and cause(s): Earth and Planetary Science Letters, v. 297, p. 298–305, https://doi.org/10.1016/j.epsl.2010.06.031.

Dameron, S.N., Leckie, R.M., Clark, K., MacLeod, K.G., Thomas, D.J., and Lees, J.A., 2017, Extinction, dissolution, and possible ocean acidification prior to the Cretaceous/Paleogene (K/Pg) boundary in the tropical Pacific: Palaeogeography, Palaeoclimatology, Palaeoecology, v. 485, p. 433–454, https://doi.org/10.1016/j.palaeo.2017.06.032.

D’Hondt, S., 2005, Consequences of the Cretaceous/Paleogene mass extinction for marine ecosystems: Annual Review of Ecology, Evolution, and Systematics, v. 36, p. 295–317, https://doi.org/10.1146/annurev.ecolsys.35.021103.105715.

D'Hondt, S., and Keller, G., 1991, Some patterns of planktic foraminiferal assemblage turnover at the Cretaceous-Tertiary boundary: Marine Micropaleontology, v. 17, p. 77–118, https://doi.org/10.1016/0377-8398(91)90024-Z.

Dinarès-Turell, J., Baceta, J.I., Pujalte, V., Orue-Etxebarria, X., Bernaola, G., and Lorito, S., 2003, Untangling the Palaeocene climatic rhythm: An astronomically calibrated Early Palaeocene magnetostratigraphy and biostratigraphy at Zumaia (Basque basin, northern Spain): Earth and Planetary Science Letters, v. 216, p. 483–500, https://doi.org/10.1016/S0012-821X(03)00557-0.

Dinarès-Turell, J., Westerhold, T., Pujalte, V., Röhl, U., and Kroon, D., 2014, Astronomical calibration of the Danian stage (Early Paleocene) revisited: Settling chronologies of sedimentary records across the Atlantic and Pacific Oceans: Earth and Planetary Science Letters, v. 405, p. 119–131, https://doi.org/10.1016/j.epsl.2014.08.027.

Font, E., Adatte, T., Andrade, M., Keller, G., Mbabi Bitchong, A., Carvallo, C., Ferreira, J., Diogo, Z., and Mirão, J., 2018, Deccan volcanism induced high-stress environment during the Cretaceous–Paleogene transition at Zumaia, Spain: Evidence from magnetic, mineralogical and biostratigraphic records: Earth and Planetary Science Letters, v. 484, p. 53–66, https://doi.org/10.1016/j.epsl.2017.11.055.

Gallala, N., Zaghbib-Turki, D., Molina, E., Arenillas, I., and Arz, J.A., 2009, Planktic foraminiferal catastrophic mass extinction and assemblage evolution across the Cretaceous/Paleogene (K/Pg) boundary at Bidart (SW France): Marine Micropaleontology, v. 72, p. 196–209, https://doi.org/ 10.1016/j.marmicro.2009.05.001.

Gibbs, S.J., Bown, P.R., Ward, B.A., Alvarez, S.A., Kim, H., Archontikis, O.A., Sauterey, B., Poulton, A.J., Wilson, J., and Ridgwell, A., 2020, Algal plankton turn to hunting to survive and recover from end-Cretaceous impact darkness: Science Advances, v. 6, p. eabc9123, https://doi.org/10.1126/sciadv.abc9123.

Gilabert, V., Arz, J.A., Arenillas, I., and Robinson, S.A., 2021, Influence of the Latest Maastrichtian Warming Event on planktic foraminiferal assemblages and ocean carbonate saturation at Caravaca, Spain: Cretaceous Research, v., 125, 104844, https://doi.org/10.1016/j.cretres.2021.104844.

Hilgen, F.J., Kuiper, K.F., and Lourens, L.J., 2010, Evaluation of the astronomical time scale for the Paleocene and earliest Eocene: Earth and Planetary Science Letters, v. 300, p. 139–151, https://doi.org/10.1016/j.epsl.2010.09.044.

Hilgen, F.J., Abels, H.A., Kuiper, K.F., Lourens, L.J., and Wolthers, M., 2015, Towards a stable astronomical time scale for the Paleocene: Aligning Shatsky Rise with the Zumaia - Walvis Ridge ODP site 1262 composite: Newsletters on Stratigraphy, v. 48, p. 91–110, https://doi.org/10.1127/nos/2014/0054.

Hull, P.M. et al., 2020, On impact and volcanism across the Cretaceous-Paleogene boundary: Science, v. 367, p. 266–272, https://doi.org/10.1126/science.aay5055.

Husson, D., Galbrun, B., Laskar, J., Hinnov, L.A., Thibault, N., Gardin, S., and Locklair, R.E., 2011, Astronomical calibration of the Maastrichtian (Late Cretaceous): Earth and Planetary Science Letters, v. 305, p. 328–340, https://doi.org/10.1016/j.epsl.2011.03.008.

Jiang, S., Bralower, T.J., Patzkowsky, M.E., Kump, L.R., and Schueth, J.D., 2010, Geographic controls on nannoplankton extinction across the Cretaceous/Palaeogene boundary: Nature Geoscience, v. 3, p. 280–285, https://doi.org/10.1038/ngeo775.

Jones, H.L., Lowery, C.M., and Bralower, T.J., 2019, Delayed calcareous nannoplankton boom-bust successions in the earliest Paleocene Chicxulub (Mexico) impact crater: Geology, v. 47, https://doi.org/10.1130/G46143.1.

Kuiper, K.F., Deino, A., Hilgen, F.J., Krijgsman, W., Renne, P.R., and Wijbrans, J.R., 2008, Synchronizing rock clocks of earth history: Science, v. 320, p. 500–504, https://doi.org/10.1126/science.1154339.

Laskar, J., Gastineau, M., Delisle, J.-B., Farrés, A., and Fienga, A., 2011, Strong chaos induced by close encounters with Ceres and Vesta: A&A, v. 532, p. 4, https://doi.org/10.1051/0004-6361/201117504.

Li, L., and Keller, G., 1998, Maastrichtian climate, productivity and faunal turnovers in planktic foraminifera in South Atlantic DSDP sites 525A and 21: Marine Micropaleontology, v. 33, p. 55–86, https://doi.org/10.1016/S0377-8398(97)00027-3.

Lirer, F., 2000, A new technique for retrieving calcareous microfossils from lithified lime deposits: Micropaleontology, v. 46, p. 365–369.

Lowery, C.M. et al., 2018, Rapid recovery of life at ground zero of the end-Cretaceous mass extinction: Nature, v. 558, p. 288–291, https://doi.org/10.1038/s41586-018-0163-

Molina, E., Alegret, L., Arenillas, I., and Arz, J.A., 2005, The Cretaceous/Paleogene boundary at the Agost section revisited: paleoenvironmental reconstruction and mass extinction pattern: Journal of Iberian Geology, v.31, p.135-148.

Molina, E., Alegret, L., Arenillas, I., Arz, J.A., Gallala, N., Grajales-Nishimura, J.M., Murillo-Muñetón, G., and Zaghbib-Turki, D., 2009, The Global Boundary Stratotype Section and Point for the base of the Danian Stage (Paleocene, Paleogene, "Tertiary", Cenozoic): Auxiliary sections and correlation: Episodes, v. 32, p. 84–95, https://doi.org/10.18814/epiiugs/2009/v32i2/002.

Mukhopadhyay, S., Farley, K.A., and Montanari, A., 2001, A short duration of the Cretaceous-Tertiary boundary event: Evidence from extraterrestrial ^{3}Helium: Science, v. 291, p. 1952–1955, https://doi.org/10.1126/science.291.5510.1952.

Quillévéré, F., Norris, R.D., Kroon, D., and Wilson, P.A., 2008, Transient ocean warming and shifts in carbon reservoirs during the early Danian: Earth and Planetary Science Letters, v. 265, p. 600–615, https://doi.org/10.1016/j.epsl.2007.10.040.

Renne, P., Arenillas, I., Arz, J.A., Bermúdez, H., Vadja, V., Gilabert, V., 2018, Multi-proxy record of the Chicxulub impact at the Cretaceous/Paleogene boundary from Gorgonilla Island, Colombia: Geology, v. 46, no. 6, p. 547–550, https://doi.org/ 10.1130/G40224.1.

Ruíz, F.M., Huertas, M.O., Palomo, I., and Barbieri, M., 1992, The geochemistry and mineralogy of the Cretaceous-Tertiary boundary at Agost (southeast Spain): Chemical Geology, v. 95, p. 265–281, https://doi.org/10.1016/0009-2541(92)90016-X.

Sepúlveda, J., Alegret, L., Thomas, E., Haddad, E., Cao, C., and Summons, R.E., 2019, Stable Isotope Constraints on Marine Productivity Across the Cretaceous-Paleogene Mass Extinction: Paleoceanography and Paleoclimatology, v. 34, p. 1195–1217, https://doi.org/10.1029/2018PA003442.

Schulte, P. et al., 2010, The Chicxulub asteroid impact and mass extinction at the Cretaceous-Paleogene boundary: Science, v. 327, p. 1214–1218, https://doi.org/10.1126/science.1177265.

Smit, J., 1982, Extinction and evolution of planktonic foraminifera after a major impact at the Cretaceous/Tertiary boundary: Special Paper of the Geological Society of America, v. 190, p. 329–352, https://doi.org/10.1130/SPE190-p329.

Smit, J., 1990, Meteorite impact, extinctions and the Cretaceous-Tertiary Boundary: Geologie en Mijnbouw, v. 69, p. 187–204.

Smit, J., 1999, The global stratigraphy of the Cretaceous-Tertiary boundary impact ejecta: Annual Review of Earth and Planetary Sciences, v. 27, p. 75–113, https://doi.org/10.1146/annurev.earth.27.1.75.

Smit, J., and Romein, A.J.T., 1985, A sequence of events across the Cretaceous-Tertiary boundary: Earth and Planetary Science Letters, v. 74, p. 155–170, https://doi.org/10.1016/0012-821X(85)90019-6.

ten Kate, W.G.H.Z., and Sprenger, A., 1993, Orbital cyclicities above and below the Cretaceous/Paleogene boundary at Zumaya (N Spain), Agost and Relleu (SE Spain): Sedimentary Geology, v. 87, p. 69–101, https://doi.org/10.1016/0037-0738(93)90037-6.

Voigt, S., Gale, A.S., Jung, C., and Jenkyns, H.C., 2012, Global correlation of upper Campanian- Maastrichtian successions using carbon-isotope stratigraphy: Development of a new Maastrichtian timescale: Newsletters on Stratigraphy, v. 45, p. 25–53, https://doi.org/10.1127/0078-0421/2012/0016.

Wade, B.S., Pearson, P.N., Berggren, W.A., and Pälike, H., 2011, Review and revision of Cenozoic tropical planktonic foraminiferal biostratigraphy and calibration to the geomagnetic polarity and astronomical time scale: Earth-Science Reviews, v. 104, p. 111–142, https://doi.org/10.1016/j.earscirev.2010.09.003.

Westerhold, T., Röhl, U., Raffi, I., Fornaciari, E., Monechi, S., Reale, V., Bowles, J., and Evans, H.F., 2008, Astronomical calibration of the Paleocene time: Palaeogeography, Palaeoclimatology, Palaeoecology, v. 257, p. 377–403, https://doi.org/10.1016/j.palaeo.2007.09.016.

Woelders, L. et al., 2017, Latest Cretaceous climatic and environmental change in the South Atlantic region: Paleoceanography, v. 32, p. 466–483, https://doi.org/10.1002/2016PA003007.